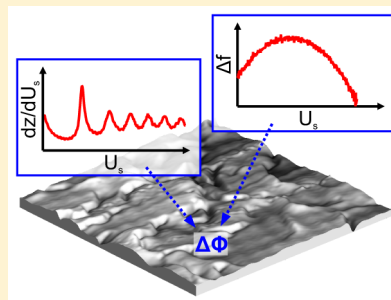


# MgO on Mo(001): Local Work Function Measurements above Pristine Terrace and Line Defect Sites

Stefanie Stuckenholtz, Christin Büchner, Markus Heyde,\* and Hans-Joachim Freund

Fritz-Haber-Institut der Max-Planck-Gesellschaft, Faradayweg 4-6, 14195 Berlin, Germany

**ABSTRACT:** We present a local spectroscopy study of thin MgO films on Mo(001), investigated with a combined noncontact atomic force microscope (nc-AFM) and scanning tunneling microscope (STM). The work function of Mo(001) and MgO/Mo(001) was measured with field emission resonance (FER) spectroscopy. The work function of the clean Mo(001) surface  $\Phi_{\text{Mo}}$  was determined to be 4.5 eV. After the deposition of an 8 atomic layer thick MgO film, it decreased to  $\Phi_{\text{MgO/Mo}} = 3.2$  eV ( $\Delta\Phi_{\text{FER}} = -1.3$  eV). This work function shift  $\Delta\Phi_{\text{FER}}$  introduced by the oxide film on the metal work function, was also investigated with contact potential difference (CPD) measurements. Here, a lowering of the work function by  $\Delta\Phi_{\text{CPD}} = -1.1$  eV was measured. Furthermore, the influence of line defects, present in the MgO film, on the local work function was investigated and compared to pristine terrace sites of the oxide film. Here, we measured a slightly higher local work function of +200 meV above line defects as compared to pristine oxide terrace sites.



## INTRODUCTION

Thin oxide films are widely used in communication technology,<sup>1</sup> energy production,<sup>2</sup> and heterogeneous catalysis.<sup>3</sup> Metal supported thin oxide films are used as model systems for heterogeneous catalysis to study elementary processes, such as electron transfer between the substrate and adsorbates.<sup>4</sup> A conductive metal support does not only enable surface science studies of the insulating oxides, the interaction between the thin oxide film and the metal support also leads to a change of the electronic and structural properties as compared to the pristine materials.<sup>1,5</sup>

MgO is a widely studied model system in heterogeneous catalysis. In recent years, a greater interest in the electron trapping properties of structural elements, such as point defects, line defects, and grain boundaries, has arisen.<sup>6,7</sup> The importance of electron trapping sites in MgO has already been studied with MgO/Ag(001) for point defects.<sup>8</sup> Studies on the growth behavior of MgO on Mo(001) have shown that the lattice mismatch between MgO and the Mo(001) substrate leads to the formation of line defects in the oxide to minimize tension, making this sample system ideal to study the influence of line defects on the local electronic structure.<sup>9,10</sup>

An important quantity for the electron transfer is the work function  $\Phi$  of a system. Oxide films can introduce a shift to the metal work function. This work function shift ( $\Delta\Phi$ ) varies locally depending on structural features, such as point defects<sup>11,12</sup> or line defects.<sup>13</sup>

There are several possibilities to measure  $\Delta\Phi$  for thin film systems. Photo emission-based spectroscopy techniques measure the kinetic energy of extracted electrons. This could be photo emission spectroscopy (PES),<sup>14</sup> an integrative method averaging over several  $\text{mm}^2$  of the sample,<sup>15</sup> or photo emission electron microscopy (PEEM), a semilocal measurement.<sup>16</sup> A local scanning probe method that can be

used for work function analysis is based on field emission resonances, using standing electron waves between sample and tip.<sup>17,18</sup> The Kelvin method, developed by Lord Kelvin,<sup>19</sup> is based on electrostatics. It measures the contact potential difference between the sample and the probe, enabling measurements of work function shifts ( $\Delta\Phi$ ). This method can be used as an integrative technique or as a local technique in Kelvin probe force microscopy (KPFM), where imaging and local measurements on the scale of nanometers are possible, even of bulk oxides.<sup>12,20</sup> The local methods enable direct measurements of  $\Delta\Phi$  above structural features, such as defects and electron trapping sites.<sup>8,21</sup>

For this article, the electronic surface structure of MgO/Mo(001) was studied with the local probing method of combined nc-AFM and STM. The metal work function reduction  $\Delta\Phi$  induced by MgO thin films on Mo(001) was investigated, and the measurements are compared to results of other experimental techniques<sup>15,22,23</sup> and theoretical work,<sup>24–27</sup> as well as MgO-induced shifts on a different substrate, Ag(001).<sup>11,28,29</sup>

Discrepancies between the theoretical and experimental results for MgO/Mo(001) are discussed with respect to the defect-rich morphology of MgO thin films grown on Mo(001) in comparison to defect-poor films grown on the substrate Ag(001), where theory and experiment agree well. Local measurements of the electronic structure above line defects and pristine MgO terrace sites were performed to elucidate the role of these structural features for  $\Delta\Phi$ .

**Received:** December 17, 2014

**Revised:** April 30, 2015

**Published:** May 8, 2015

## EXPERIMENTAL SECTION

The sample preparation and the experiments were performed in one ultrahigh vacuum (UHV) system. The system is equipped with standard tools for thin film preparation and a combined nc-AFM and STM microscope that is operated at low temperatures (5 K).

The single crystal Mo(001) substrate was cleaned by cycles of annealing in oxygen atmosphere ( $p_{O_2} = 5 \times 10^{-7}$  mbar, 15 min), of Ar-sputtering at 1.5 keV ( $p_{Ar} = 1 \times 10^{-5}$  mbar, 60 min), followed by flashing the sample to 1450 and 2100 K, respectively. Mg was evaporated from a Knudsen cell in an oxygen atmosphere ( $p_{O_2} = 5 \times 10^{-7}$  mbar) onto the Mo(001) single crystal support at room temperature to achieve a film thickness of 8 atomic layers (8 ML). After film deposition, the sample was annealed at 1170 K for 10 min in UHV.

The Mg evaporator flux is controlled with the internal flux monitor of the evaporator. The flux monitor is calibrated by evaporation of Mg on a bare metal surface, using the STM to detect a submonolayer coverage.

The microscope is operated at low temperatures to reduce damping of the tuning fork sensor, to enhance tip stability, and to minimize piezo hysteresis, piezo drift, and thermal drift. The detailed quartz tuning fork sensor design can be found elsewhere.<sup>30,31</sup> nc-AFM and STM can be used at the same surface position with a full metal Pt<sub>0.9</sub>/Ir<sub>0.1</sub>-tip. The resonance frequency shift of the tuning fork and the tunneling current can be acquired simultaneously. In the used setup, the sample is biased during measurements.

Work function shifts were determined with two different methods, field emission resonance (FER) and contact potential difference (CPD) measurements. A schematic showing the potential between tip and sample for the case of FER and CPD measurements is presented in Figure 1.

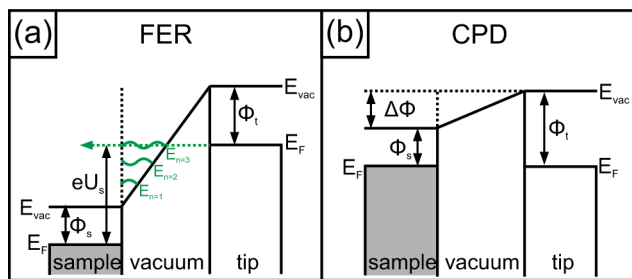


**Figure 1.** Schematics showing the potential between sample and tip (a) for bias applied larger than the work function of the sample. Here, electrons can form standing waves in the vacuum gap between tip and sample at certain field emission resonance energies. Schematics showing the potential between sample and tip (b) for contact potential difference measurements. In the sketched case, tip and sample are electrically connected, and the Fermi levels are aligned resulting in an electrostatic field due to the work function difference. The sample bias at which the electrostatic field is compensated corresponds to the contact potential difference:  $U_{CPD} = (\Phi_s - \Phi_t)/e$ .

With field emission resonance spectroscopy, we obtain information about the work function of the studied system. If a bias voltage exceeding the sample work function is applied, the electrons can enter the vacuum gap between tip and sample. Field emission resonances can be pictured as standing electron waves in the vacuum gap between tip and sample. An energy

diagram describing this situation is sketched in Figure 1a. FER are also known as Gundlach oscillations.<sup>17</sup>

FER can be measured by sweeping the bias voltage and detecting the corresponding conductivity  $dI/dU$ . However,  $dz/dU$  is more straightforward to measure, and high tunneling currents between sample and tip are avoided. Here, the bias voltage is tuned and the tunneling current is kept constant with the feedback, which results in a retraction of the tip. Examples for FER measurements are given in Figure 2a. The numbers

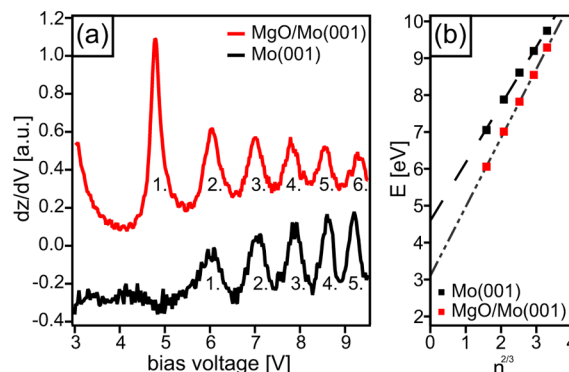


**Figure 2.** (a) Field emission resonance curves measured on Mo(001) (black line) and MgO/Mo(001) (red line). The numbers indicate the resonance numbers  $n$ . The feedback was on  $I(z)$  during the measurements. (b) Example of a plot with FER peak energy position  $E$  versus  $n^{2/3}$  for work function analysis. The sample work function can be extracted from the intersection of the fit (dashed lines) with the energy axis.

indicate the corresponding resonance number  $n$  of each peak. For data analysis, a one-dimensional tunnel junction between sample and tip is assumed, where FER develop under the following condition:<sup>32</sup>

$$eU_n = \Phi + \left( \frac{3\pi\hbar e}{2\sqrt{2m}} \right)^{2/3} F^{2/3} n^{2/3} \quad (1)$$

with the charge of an electron  $e$ , the applied sample voltage  $U_n$  of the resonance with the number  $n$ , and  $F$  the electric field between tip and sample. With eq 1, we can determine the energy to extract an electron from the surface to the vacuum (i.e., the sample work function  $\Phi$ ). Figure 2b shows a plot of the resonance peak energy versus  $n^{2/3}$ ; the sample work function can be extracted from the intersection of the fit (dashed lines) with the energy axis, according to eq 1. Because of image charge effects, the first resonance peak position is neglected for the work function analysis. During the FER measurements, the tuning fork oscillation amplitude is turned off to enter a static mode of tunneling current detection, as opposed to a dynamic mode.<sup>33</sup>

The work function shift  $\Delta\Phi$  between tip and sample was also determined with contact potential difference (CPD) measurements based on Kelvin probe force microscopy (KPFM). When two metals with different work functions are in electrical contact with each other, see Figure 1b, the Fermi levels are aligned resulting in an electrostatic field. The sample bias at which the electrostatic field is compensated corresponds to the contact potential difference. The CPD is related to the work functions of tip  $\Phi_t$  and sample  $\Phi_s$ ,  $U_{CPD} = (\Phi_s - \Phi_t)/e$ . By measuring the CPD of two samples ( $U_{CPD1}$  and  $U_{CPD2}$ ) with

the same tip, the work function difference between these samples, which equals  $\Delta\Phi$ , can be attained; see eq 2.

$$e(U_{\text{CPD2}} - U_{\text{CPD1}}) = (\Phi_{\text{s2}} - \Phi_{\text{t}}) - (\Phi_{\text{s1}} - \Phi_{\text{t}}) = \Delta\Phi \quad (2)$$

An example of CPD measurements can be found in Figure 3. The frequency shift versus bias voltage measurements show a

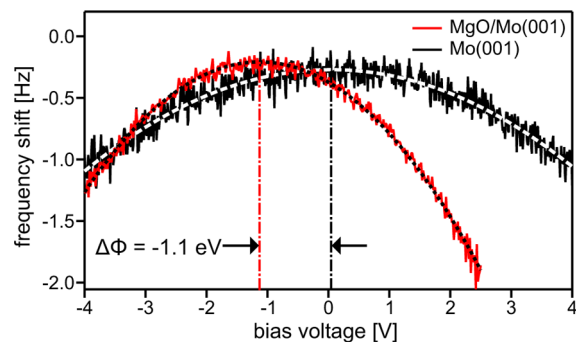


**Figure 3.** Local contact potential difference measurements on clean Mo(001) (black line, dashed parabola fit) and on 8 ML MgO/Mo(001) (red line, dotted parabola fit). The tip–sample distance was constant during the measurements. The work function shift is indicated by the vertical dashed-dotted lines and arrows.

parabolic behavior, caused by the long-range electrostatic forces acting between the tip and the sample.<sup>34</sup> At the voltage of the CPD, the frequency shift signal shows the maximum frequency shift position, indicating minimal Coulomb forces between the tip and the probed sample area. During each measurement, the tip–sample distance was constant. At the same time the amplitude was constant, so an amplitude-induced change of the frequency shift can be excluded.

The work function and the contact potential differences of an 8 ML MgO/Mo(001) sample and of a clean Mo(001) surface were measured on different positions on the sample surface, with FER and with CPD, respectively.

The area above a line defect and the area above a terrace site of an 8 ML MgO/Mo(001) film were also investigated with CPD measurements for local  $\Delta\Phi$  investigations.

## RESULTS AND DISCUSSION

The work function shift was determined between a Mo(001) surface and MgO thin films on Mo(001). For this we measured the sample work function with FER spectroscopy and the contact potential difference with CPD on cleaned Mo(001) and on MgO/Mo(001) terrace sites. To make a statement about the sample work function shift, the measurements were performed on several different positions on the sample surface. With this statistical approach, the effect of tip and local sample variations on the resulting overall values is minimized. The data of both methods show a standard deviation of about 0.2 eV.

The work function shift between terrace and line defect sites of 8 ML MgO/Mo(001) was studied to investigate how these structural elements influence  $\Delta\Phi$ . The same positions were measured several times at various tip–sample distances to investigate the influence of the line defects on the local work function as a function of the tip–sample distance. The tip configuration can influence the tip work function and the imaging contrast. We used this correlation to confirm tip stability before and after spectroscopy. The maxima of the CPD

data that were measured in direct succession show a standard deviation of 20 meV.

The results are compared to experimental and theoretical data from the literature.

**Work Function Shift Induced by MgO on Mo(001).** STM images of a cleaned Mo(001) substrate and of an 8 ML thick MgO film on Mo(001) are shown in Figure 4a and b,

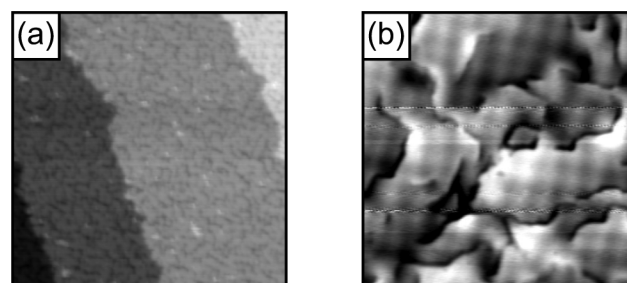


**Figure 4.** STM image (a) of bare Mo(001) recorded with a bias voltage  $U_s = 1$  V and a tunneling current set point  $I_t = 100$  pA. The image size is  $50 \times 50$  nm<sup>2</sup>. STM image (b) of an 8 ML thick MgO film on Mo(001) recorded with a bias voltage  $U_s = 4.5$  V and a tunneling current set point  $I_t = 100$  pA. The image size is  $80 \times 80$  nm<sup>2</sup>.

respectively. The Mo(001) substrate shows monoatomic stepped terraces. The MgO surface exhibits a closed, flat oxide film with some prominent structural features. A number of point defects and line defects are visible. A feature that is found over the whole surface is a moiré-like pattern. It is only imaged at certain voltages for thicker films. The moiré-like pattern has been thoroughly described in the literature.<sup>9</sup> Here, it is assumed that the first layers of the film exhibit rumpling effects as a compensation for the mismatch between the Mo and the MgO lattices of 5.8% at the interface.<sup>35</sup> In thicker films, as used here, the mismatch is compensated by the introduction of structural elements, such as screw dislocations and step dislocations, visible as line defects at the sample surface and mosaic formation. The morphology of MgO films on Mo(001) is schematically illustrated in Figure 5a. As a comparison, the morphology of thin MgO films on Ag(001) is illustrated in Figure 5b. Here, smooth layer-by-layer growth of defect-poor thin oxide films can be achieved. No line defects are present, due to the smaller mismatch of 2.9% between Ag(001) and MgO.<sup>35</sup> MgO islands sinking into the Ag substrate have been reported, and under certain growth conditions, mosaic formation is possible.<sup>35–38</sup>

Figure 5c and d illustrate two known mechanisms that contribute to  $\Delta\Phi$  of the metal support work function upon the deposition of an oxide film. In Figure 5c the electron density  $\rho(z)$  that spills out of the surface into the vacuum is sketched. This electron spill-out creates a surface dipole, which is the origin of the work function. When a dielectric layer, such as the oxide film, is deposited, the electron spill-out is reduced because of Coulomb repulsion. This causes a reduction of the work function. The reduction gets larger with a decrease of the distance between the substrate and the oxide layer. Another effect that has an influence on  $\Delta\Phi$  is the interfacial charge transfer between a dielectric layer and a metal substrate; it is sketched in Figure 5d. There can be electron transfer from the metal to the oxide, resulting in a shift to higher work functions ( $\Delta\Phi > 0$ ), or electrons can be transferred from the oxide to the metal ( $\Delta\Phi < 0$ ).

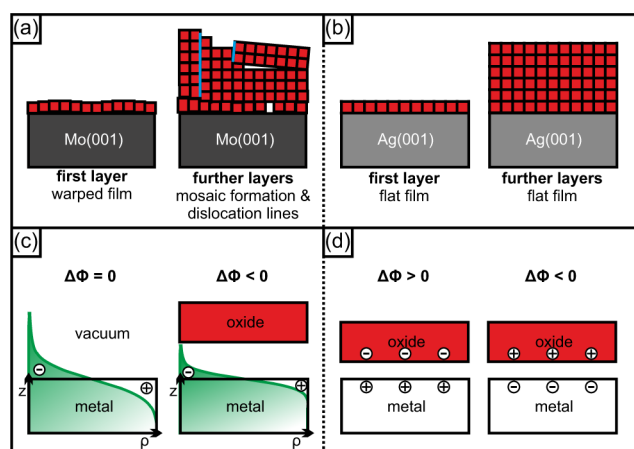


**Figure 5.** (a and b) Schematics of MgO (red) thin film morphology on different supports (gray): (a) Mo(001) substrate, showing a moiré-like structure (i.e., a warped thin film) for the first layer and dislocations (blue) as well as mosaic formation in thicker film layers; and (b) Ag(001) substrate, exhibiting flat and defect-poor film morphology. (c and d) Schematics illustrating different mechanisms that contribute to the work function shift of a metal support after the deposition of an oxide film. (c) The electron density  $\rho(z)$  spills out of the metal surface into the vacuum, creating a surface dipole normal to the surface. The Coulomb repulsion of an oxide layer reduces the electron density spill over; hence the work function  $\Phi$  is reduced. (d) A charge transfer at the interface between the metal support and the oxide film can also contribute to a work function shift  $\Delta\Phi$ .

Theoretical calculations indicate that there is some charge transfer from MgO films to the metal substrate at the interface and that interface rumpling also occurs, which is interconnected with the charge transfer.<sup>27</sup> Yet theoretical calculations also show that for highly ionic materials, such as MgO, the work function shift is mainly due to Coulomb repulsion.<sup>25,26</sup>

In different areas over the sample surface, we determined  $\Phi$  and  $\Delta\Phi$  with FER and with CPD as described in the previous section. With FER, we determined the work function values of the Mo(001) substrate  $\Phi_{\text{Mo}} = 4.5$  eV and for the 8 ML MgO/Mo(001) sample  $\Phi_{\text{MgO/Mo}} = 3.2$  eV, resulting in a work function shift  $\Delta\Phi_{\text{FER}}$  of  $-1.3$  eV. The measured value of the Mo(001) work function is in good agreement with other experimental data from the literature, for example, 4.53 eV measured with the photoelectric Fowler method.<sup>39</sup> With CPD, a work function shift  $\Delta\Phi_{\text{CPD}} = -1.1$  eV was determined.

The results are listed in Table 1 and compared to values from the literature. As a comparison, the data from experiments and theory are also denoted for another sample system, MgO/Ag(001). The measurements in this work on MgO/Mo(001) and Mo(001) were performed with the same machine as measurements on MgO/Ag(001) and Ag(001) by König et al.<sup>11</sup> The theoretical calculations cited are based on density functional theory (DFT).

Table 1 lists results of experimental and theoretical work on work function shift values induced by the indicated number of MgO layers with respect to the metal support work function. The first column presents the studied sample system, and the second column indicates the thickness of the MgO film in monolayers. The third column shows the resulting  $\Delta\Phi = \Phi_{\text{MgO/metal}} - \Phi_{\text{metal}}$ , acquired with the corresponding technique listed in column four. The corresponding references are listed in column five.

**Table 1. Comparison of Experimental and Theoretical Data<sup>a</sup>**

sample system	number of layers	$\Delta\Phi$ [eV]	method	ref	
MgO/Mo(001)	8	-1.3	FER	this work	
	8	-1.1	CPD	this work	
	3–10	-1.24	PES	15	
	7	-1.5	FER	23	
	~10	-1.0	MIES	22	
	2	-1.82	DFT	26	
	3	-1.74	DFT	25	
	3	-2.14	DFT	24	
	MgO/Ag(001)	2–5	-1.4	UPS	28
		8–10	-1.1	UPS	28
2		-1.4	KPFM	29	
3		-1.3	FER	11	
3		-1.1	CPD	11	
3		-2.08 to $-0.98^b$	DFT	27	
2		-1.22	DFT	26	
3		-1.27	DFT	25	
3		-1.18	DFT	24	

<sup>a</sup>Work function shift values induced by the indicated number of MgO layers with respect to the metal support work function. <sup>b</sup>Different van der Waals corrected DFT methods.

The results of measurements with the two local techniques CPD and FER of this work are in good agreement. The larger shift measured with FER was also observed by König et al. for the system MgO/Ag(001).<sup>11</sup> Our findings support the measurements by Vaida et al.<sup>15</sup> acquired with femto-second laser photo emission spectroscopy, a technique integrating over an area of 2 mm<sup>2</sup> of the sample surface. They studied the evolution of the work function with respect to the oxide layer thickness. The maximum value for  $\Delta\Phi$  was measured for 3 ML and thicker oxide films. Benia et al.<sup>23</sup> estimated the work function shift between a clean Mo(001) and a sample with 7 ML MgO/Mo(001) to be  $-1.5$  eV from the shift of the first FER peaks. Krischok et al.<sup>22</sup> report a decrease of the work function of about 1.0 eV during the preparation of approximately 2 nm thick MgO films on clean Mo(001). For the in situ study of the work function, they used metastable impact electron spectroscopy (MIES).

The experimentally observed values for  $\Delta\Phi$  vary over a wide range and lie between  $-1.0$  and  $-1.5$  eV. Theoretical calculations for the system MgO/Mo(001),<sup>24–26</sup> all from the Pacchioni group, predict a higher shift than all of the experimentally observed values.

The lower part of Table 1 lists experimental and theoretical results for  $\Delta\Phi$  of MgO on Ag(001). Jaouen et al.<sup>28</sup> found in an ultraviolet photo electron spectroscopy (UPS) study a shift of  $-1.4$  eV for films with a thickness between 2 and 5 ML and a slightly reduced shift of  $-1.1$  eV for films with a thickness of 8–10 ML. A 2 ML thick MgO film on Ag(001) was studied with Kelvin probe force microscopy (KPFM) by Bielecki et al.,<sup>29</sup> and they found a  $\Delta\Phi$  of  $-1.4$  eV. These findings agree well with the local SPM studies of König et al. on 3 ML thick films. The experimental results are in the range of  $-1.4$  to  $-1.1$  eV for MgO/Ag(001).

Calculations similar to those for MgO/Mo(001) were performed by the Pacchioni group for MgO on a Ag(001) substrate.<sup>24–26</sup> Here, the values agree well with the experimental findings of an integrative and a local spectroscopy

technique. Variations of the computed values with the same code and the same functionals can be assigned to variations of calculation details, for example, the number of metal layers used to simulate the metal support, or the reciprocal space sampling employed.

A new theoretical study by Ling et al.<sup>27</sup> compared the performance of different van der Waals corrected density functional methods and functionals on calculating the interface geometry and  $\Delta\Phi$  for MgO/Ag(001). They could show that including the van der Waals interaction is important for obtaining accurate interface structures and work function shifts. Even small changes in the interface geometry strongly affected  $\Delta\Phi$ .

Pal et al. recently investigated the influence of excess interfacial oxygen on the work function of MgO/Ag(001).<sup>40</sup> The charge transfer from the substrate to the electronegative oxygen leads to the formation of a surface dipole, which increases the work function.<sup>40</sup> The presence of excess oxygen at the interface or the accumulation at defects can not be excluded and could be a further explanation for differences in the resulting work function shift of theoretical work and experimental studies.

Despite their similar work functions, the different characteristics of Ag(001) and Mo(001) can be used to explain the good match between the theoretical and experimental data for the system MgO/Ag(001), versus the discrepancy for the system MgO/Mo(001). One possible reason for this gap are the structural differences, arising from the larger lattice mismatch between MgO and Mo(001) as compared to MgO and Ag(001). The growth behavior of MgO differs on the two substrates, as already discussed. MgO is contracted and shows rumpling to fit to the smaller Mo(001) lattice. On the other hand, the MgO film is slightly stretched to adapt to the Ag(001) lattice parameter. This indicates a complex interface structure in the case of MgO/Mo(001), which is not easy to model by theory. As shown by Ling et al.,<sup>27</sup> small changes of the interface structure in the model lead to large changes in the resulting values.

An accumulation of excess negative charges in the reported line defects (not only at the interface between the metal substrate and MgO film) is also a possible explanation for the smaller work function shift of MgO/Mo(001) in the experiments. The preparation conditions of the MgO films, Mg evaporation in oxygen atmosphere, make it possible for interfacial oxygen to be present between the oxide and the Mo(001).

Overall, there are various factors that influence the resulting  $\Phi$  of the sample system MgO/Mo(001). The effects at the interface between oxide film and metal substrate (charge transfer, electron spill out), possible excess interfacial oxygen, as well as defects in the oxide film appear to have a strong influence on the sample work function. To contribute to the important and ongoing discussion about this topic with our setup, we investigated line defects on the atomic scale. An investigation comparing the local electronic structure above line defects to pristine oxide terrace sites follows in the next section.

**Line Defects in MgO/Mo(001).** CPD measurements were performed above line defects and above pristine terrace sites on an 8 ML thick MgO film on a Mo(001) substrate. STM images of the probed area are shown in Figure 6. Figure 6a shows a typical overview image of a thin MgO film on Mo(001). A flat oxide film terrace with several line defects is visible. A close-up image of the probed area is shown in Figure 6b. The blue and

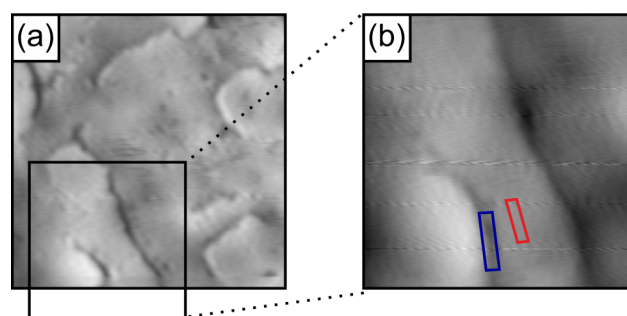


**Figure 6.** STM images of 8 ML MgO on Mo(001) recorded with a bias voltage of +4.2 V and a tunneling current set point of 10 pA. (a) The image size is 35 nm  $\times$  35 nm. A closed, flat oxide film with point defects and line defects can be seen. (b) The image size is 20 nm  $\times$  20 nm. The image covers partly the area of image (a), as indicated by the dotted lines. The colored boxes indicate the positions over which point spectroscopy was performed. The blue box frames the investigated part of a line defect, and the red box frames the studied pristine MgO terrace area.

red boxes encircle the areas above which we performed the spectroscopy measurements of the line defect sites and the terrace sites, respectively.

Figure 7 shows two representative CPD measurements, the red one taken above a terrace site, the blue one taken above a

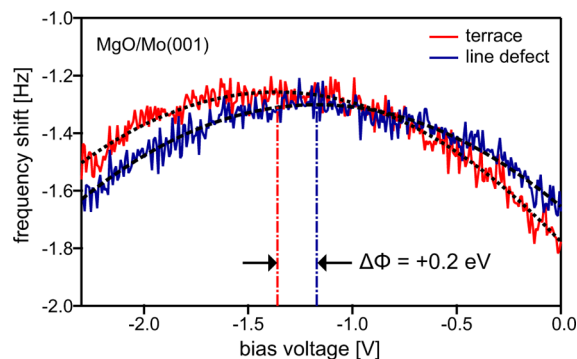


**Figure 7.** Local contact potential difference measurements on an 8 ML MgO thin film on Mo(001). The measurements were performed on a terrace site (red line, dotted parabola fit) and on a line defect site (blue line, dashed parabola fit). The tip-sample distance was constant during the measurements. The work function shift is indicated by the colored dashed-dotted lines and the arrows.

line defect site. The position of the measured CPD is indicated by colored dashed-dotted lines in the graph to guide the eye. The CPD of the line defect is shifted to higher values as compared to the terrace site CPD. Hence, the  $\Delta\Phi$  is smaller above line defects than above pristine terrace sites. In other words, a higher work function is measured above line defects as compared to terrace sites, which indicates that the line defects can act as electron trapping sites. This observation supports measurements of this defect type in MgO/Mo(001) by optical scanning tunneling spectroscopy (STS) and electron paramagnetic resonance (EPR) measurements.<sup>7,41</sup> Here, local light emission spectra acquired above line defects before and after applying a bias ramp to the sample and EPR spectra of films after exposure to hydrogen atoms indicated electron trapping in thicker MgO films. A defect state at  $-3.3$  eV was found with STS at line defect sites.<sup>7</sup>

In Figure 8, the measured CPD values above a terrace site (red) and of a line defect site (blue) are presented in the form

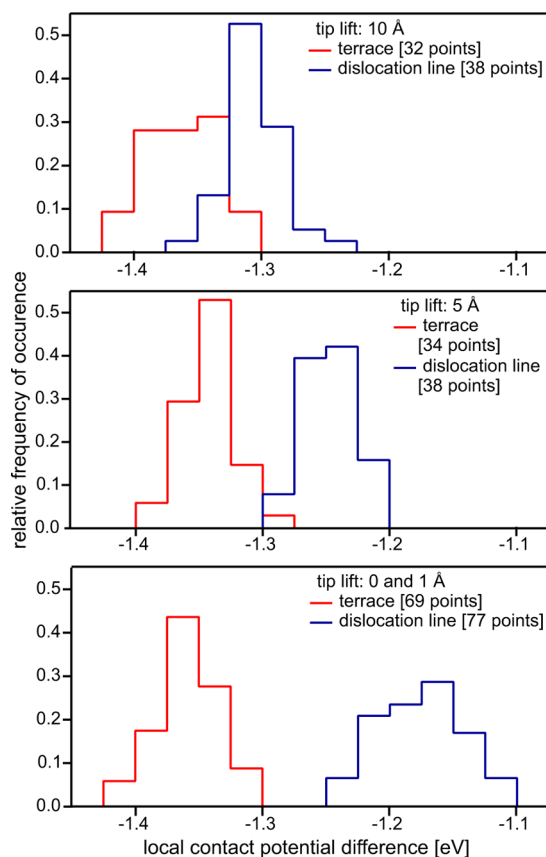


**Figure 8.** Histograms of the local contact potential difference above pristine MgO terrace sites (red line) and above line defect sites (blue line) for different tip retractions, as indicated. The bin size is 25 meV. The data are derived from measurements above the sites marked with rectangles in Figure 6b. The corresponding tip lift during the measurements and the number of data points contributing to the histograms are given in the top right corner of each histogram.

of a histogram. The CPD measurements were performed with different tip retractions. The CPD values above the terrace site are not significantly affected by the  $z$ -displacement. The CPD above the line defect site is shifted to larger values as the tip approaches. The stronger divergence of the CPD for the terrace and for the line defect sites upon lowering the tip closer to the surface is a sign for an increasing lateral resolution of the CPD measurement. Note that the  $z$ -axis zero value is set as the tip position above a terrace site at a bias voltage of  $U_s = -1.2$  V and a frequency shift set point of  $df = -1.25$  Hz. To exclude the influence of surface protrusions, such as neighboring steps, on the measured  $\Delta\Phi$ , the data points were measured in two different modes. During the first mode, the tip was stabilized at one point and the whole measurement series was measured in constant height, while in the second mode, the tip was stabilized above every single point, individually. Upon comparison of the results, no difference in the CPD values could be detected. Despite a limitation of the measuring range from  $-2.3$  to  $+0.7$  V, tip changes occurred during sweeping the bias voltage at closer distances between the tip and the sample surface.

The same measurements were also performed with FER, but especially at the defect sites the measurement often leads to

changes of the tip, which also indicates a higher reactivity of the line defect sites as compared to the terrace sites with metal adsorbates, such as the tip material.

In the following discussion, all values are given with reference to pristine MgO terrace site measurements on the respective support. The resulting maximum measured work function increase above the line defects is about  $+200$  meV. CPD measurements above similar sites of the same and of comparable samples were in the range from  $+100$  to  $+200$  meV, all on MgO/Mo(001) films. These values can be compared to the work function shift measurements above single point defects on 3 and 6 ML MgO thin films on Ag(001) measured with the same technique and apparatus.<sup>8</sup> In case of a positively charged  $F^{2+}$ -center (oxygen vacancy without trapped electrons), a local work function decrease of about  $-30$  meV was measured. The local work function changes are caused by changes of the local charge distribution by the surface defects. A dipole moment is induced by localized charges at the surface defect and the screening charges in the metal substrate. Electron-rich defects, such as a single  $F^0$ -center (oxygen vacancy with two trapped electrons) or a negatively charged divacancy (neighboring oxygen and magnesium vacancies with one trapped electron), increase the work function about  $+20$  and  $+40$  meV, respectively. Here, the electron charge density spills out of the defect, inducing a dipole moment that increases the local work function.<sup>42</sup>

In analogy to the point defects, the change of the local work function can be explained by electron trapping characteristics of line defects, increasing the local surface dipole and thus increasing the work function. The different magnitudes, in which point defects and line defects influence the local work function, can be explained either by a higher number of charges present or by its larger spacial dimensions. Because excess oxygen at the interface between MgO and the metal substrate can have a great influence on the work function of the system, the presence of excess oxygen in the dislocation lines could explain the higher local work function measured above them.<sup>40,43</sup>

Because of the finite curvature of the tip, the forces acting on the tip are averaged above a larger area than only the defect site in the center. The resolution as a function of the tip-sample distance has been modeled and already discussed elsewhere.<sup>8</sup> This averaging nature of the tip leads to an underestimation of the difference between the CPD values of the line defect and the terrace sites. Hence, we assume that the absolute values of  $\Phi$  above the defect sites are higher than the presented values measured with the here used local CPD technique.

Local scanning probe spectroscopy using FER and optical spectroscopy detected an increase of the local work function of  $\sim 0.7$  eV above line defect sites compared to terrace sites in a MgO/Mo(001) thin film.<sup>7</sup> The same work also proved the existence of unpaired electrons in trapping sites for these films. Here the trapping depth (energy needed for electron excitation from the trapped state to the conduction band onset) was thermally estimated to be in the order of 1.0 eV. These findings are in line with the trapping depth calculated with DFT for structural elements present in MgO grain boundaries.<sup>44</sup> As already discussed in theory, line defect sites are very promising structural elements for an increased reactivity for heterogeneous catalysts.<sup>21,45</sup>

The local work function shifts observed above the line defects can help to explain the gap between the theoretical

predictions of  $\Delta\Phi$  in the case for MgO/Mo(001), as compared to MgO/Ag(001), where these line defects are not present.

## CONCLUSION

The investigation of the local electronic surface structure of MgO/Mo(001), with FER and CPD measurements, confirmed the findings of other local and integrative methods from literature. The deviations from available data from theory were explained by the presence of line defects in the oxide films and features at the interface between oxide and metal, present in the real sample, but not taken into account by the calculations.

The influence of line defects on the local work function of MgO/Mo(001) was investigated for the first time experimentally with an AFM-based method. Local CPD measurements revealed a shift to higher work function values above line defects in comparison to pristine terrace sites in MgO/Mo(001). This strengthens the postulation that line defect sites act as electron traps in oxides and hence affect the work function shift that the oxide film introduces to the metal substrate. Still, open questions remain. Especially the role of the oxide–metal interface on the work function shift is not fully understood, yet. Further research on this topic is needed. In future experiments, it is planned to investigate the stability of line defects and their interaction with adsorbates.

## AUTHOR INFORMATION

### Corresponding Author

\*E-mail: heyde@fhi-berlin.mpg.de.

### Notes

The authors declare no competing financial interest.

## ACKNOWLEDGMENTS

We thank G. Pacchioni for fruitful discussions, G. Thielsch for technical support, and K. Burson for proofreading. We acknowledge support from the DFG through the Cluster of Excellence UNICAT.

## REFERENCES

- (1) Giordano, L.; Pacchioni, G. Oxide Films at the Nanoscale: New Structures, New Functions, and New Materials. *Acc. Chem. Res.* **2011**, *44*, 1244–1252.
- (2) Evans, A.; Bieberle-Hütter, A.; Rupp, J. L. M.; Gauckler, L. J. Review on Microfabricated Micro-solid Oxide Fuel Cell Membranes. *J. Power Sources* **2009**, *194*, 119–129.
- (3) Ertl, G.; Freund, H.-J. Catalysis and Surface Science. *Phys. Today* **1999**, *52*, 32–38.
- (4) Freund, H.-J. Model Studies in Heterogeneous Catalysis. *Chemistry* **2010**, *16*, 9384–9397.
- (5) Sterrer, M.; Risse, T.; Heyde, M.; Rust, H.-P.; Freund, H.-J. Crossover from Three-dimensional to Two-dimensional Geometries of Au Nanostructures on Thin MgO(001) Films: A Confirmation of Theoretical Predictions. *Phys. Rev. Lett.* **2007**, *98*, 6–9.
- (6) McKenna, K. P.; Shluger, A. L. First-principles Calculations of Defects Near a Grain Boundary in MgO. *Phys. Rev. B* **2009**, *79*, 224116.
- (7) Benia, H.-M.; Myrach, P.; Gonchar, A.; Risse, T.; Nilius, N.; Freund, H.-J. Electron Trapping in Misfit Dislocations of MgO Thin Films. *Phys. Rev. B* **2010**, *81*, 241415.
- (8) König, T.; Simon, G. H.; Rust, H.-P.; Pacchioni, G.; Heyde, M.; Freund, H.-J. Measuring the Charge State of Point Defects on MgO/Ag(001). *J. Am. Chem. Soc.* **2009**, *131*, 17544–17545.
- (9) Benedetti, S.; Torelli, P.; Valeri, S.; Benia, H.; Nilius, N.; Renaud, G. Structure and Morphology of Thin MgO Films on Mo(001). *Phys. Rev. B* **2008**, *78*, 195411.

(10) Benedetti, S.; Stavale, F.; Valeri, S.; Noguera, C.; Freund, H.-J.; Goniakowski, J.; Nilius, N. Steering the Growth of Metal Ad-particles via Interface Interactions Between a MgO Thin Film and a Mo Support. *Adv. Funct. Mater.* **2013**, *23*, 75–80.

(11) König, T.; Simon, G. H.; Rust, H.-P.; Heyde, M. Work Function Measurements of Thin Oxide Films on Metals - MgO on Ag(001). *J. Phys. Chem. C* **2009**, *113*, 11301–11305.

(12) Barth, C.; Henry, C. R. Kelvin Probe Force Microscopy on MgO(001) Surfaces and Supported Pd Nanoclusters. *J. Phys. Chem. C* **2009**, *113*, 247–253.

(13) Heinke, L.; Lichtenstein, L.; Simon, G. H.; König, T.; Heyde, M.; Freund, H.-J. Local Work Function Differences at Line Defects in Aluminium Oxide on NiAl(110). *ChemPhysChem* **2010**, *11*, 2085–2087.

(14) Park, Y.; Choong, V.; Gao, Y.; Hsieh, B. R.; Tang, C. W. Work Function of Indium Tin Oxide Transparent Conductor Measured by Photoelectron Spectroscopy. *Appl. Phys. Lett.* **1996**, *68*, 2699.

(15) Vaida, M. E.; Gleitsmann, T.; Tchitnga, R.; Bernhardt, T. M. Femtosecond-laser Photoemission Spectroscopy of Mo(100) Covered by Ultrathin MgO(100) Films of Variable Thickness. *J. Phys. Chem. C* **2009**, *113*, 10264–10268.

(16) Li, W. Y.; Goto, K.; Shimizu, R. PEEM is a Suitable Tool for Absolute Work Function Measurements. *Surf. Interface Anal.* **2005**, *37*, 244–247.

(17) Gundlach, K. Zur Berechnung des Tunnelstroms durch eine Trapezförmige Potentialstufe. *Solid-State Electron.* **1966**, *9*, 949–957.

(18) Binnig, G.; Frank, K.; Fuchs, H.; Garcia, N.; Reihl, B.; Rohrer, H.; Salvan, F.; Williams, A. Tunneling Spectroscopy and Inverse Photoemission: Image and Field States. *Phys. Rev. Lett.* **1985**, *55*, 991–994.

(19) Thomson (Lord Kelvin), W. Contact Electricity of Metals. *Philos. Mag. Ser. 5* **1898**, *46*, 82–120.

(20) Melitz, W.; Shen, J.; Kummel, A. C.; Lee, S. Kelvin Probe Force Microscopy and its Application. *Surf. Sci. Rep.* **2011**, *66*, 1–27.

(21) McKenna, K. P. Electronic and Chemical Properties of a Surface-terminated Screw Dislocation in MgO. *J. Am. Chem. Soc.* **2013**, *135*, 18859–18865.

(22) Krischok, S.; Stracke, P.; Höfft, O.; Kemper, V.; Zhukovskii, Y.; Kotomin, E. A Comparative Analysis of Electron Spectroscopy and First-principles Studies on Cu(Pd) Adsorption on MgO. *Surf. Sci.* **2006**, *600*, 3815–3820.

(23) Benia, H.; Nilius, N.; Freund, H.-J. Photon Mapping of MgO Thin Films with an STM. *Surf. Sci.* **2007**, *601*, L55–L58.

(24) Giordano, L.; Cinquini, F.; Pacchioni, G. Tuning the Surface Metal Work Function by Deposition of Ultrathin Oxide Films: Density Functional Calculations. *Phys. Rev. B* **2006**, *73*, 045414.

(25) Prada, S.; Martinez, U.; Pacchioni, G. Work Function Changes Induced by Deposition of Ultrathin Dielectric Films on Metals: A Theoretical Analysis. *Phys. Rev. B* **2008**, *78*, 235423.

(26) Sicolo, S.; Giordano, L.; Pacchioni, G. Adsorption of Late Transition Metal Atoms on MgO/Mo(100) and MgO/Ag(100) Ultrathin Films: A Comparative DFT Study. *J. Phys. Chem. C* **2009**, *113*, 16694–16701.

(27) Ling, S.; Watkins, M. B.; Shluger, A. L. Effects of Atomic Scale Roughness at Metal/Insulator Interfaces on Metal Work Function. *Phys. Chem. Chem. Phys.* **2013**, *15*, 19615–19624.

(28) Jaouen, T.; Jézéquel, G.; Delhayre, G.; Lépine, B.; Turban, P.; Schieffer, P. Work Function Shifts, Schottky Barrier Height, and Ionization Potential Determination of Thin MgO Films on Ag(001). *Appl. Phys. Lett.* **2010**, *97*, 232104.

(29) Bielecki, M.; Hynninen, T.; Soini, T. M.; Pivetta, M.; Henry, C. R.; Foster, A. S.; Esch, F.; Barth, C.; Heiz, U. Topography and Work Function Measurements of Thin MgO(001) Films on Ag(001) by nc-AFM and KPFM. *Phys. Chem. Chem. Phys.* **2010**, *12*, 3203–9.

(30) Rust, H.-P.; Heyde, M.; Freund, H.-J. Signal Electronics for an Atomic Force Microscope Equipped with a Double Quartz Tuning Fork Sensor. *Rev. Sci. Instrum.* **2006**, *77*, 043710.

- (31) Heyde, M.; Simon, G. H.; Rust, H.-P.; Freund, H.-J. Probing Adsorption Sites on Thin Oxide Films by Dynamic Force Microscopy. *Appl. Phys. Lett.* **2006**, *89*, 263107.
- (32) Kolesnychenko, O.; Kolesnichenko, Y.; Shklyarevskii, O.; van Kempen, H. Field-emission Resonance Measurements with Mechanically Controlled Break Junctions. *Physica B* **2000**, *291*, 246–255.
- (33) Sader, J. E.; Jarvis, S. P. Accurate Formulas for Interaction Force and Energy in Frequency Modulation Force Spectroscopy. *Appl. Phys. Lett.* **2004**, *84*, 1801.
- (34) Gross, L.; Mohn, F.; Liljeroth, P.; Repp, J.; Giessibl, F. J.; Meyer, G. Measuring the Charge State of an Adatom with Noncontact Atomic Force Microscopy. *Science* **2009**, *324*, 1428–1431.
- (35) Wollschläger, J. Morphology and Defect Characterization of Epitaxial Oxide Films. *Defect Diffus. Forum* **1998**, *164*, 37–56.
- (36) Schintke, S.; Messerli, S.; Pivetta, M.; Patthey, F.; Libiouille, L.; Stengel, M.; de Vita, A.; Schneider, W.-D. Insulator at the Ultrathin Limit: MgO on Ag(001). *Phys. Rev. Lett.* **2001**, *87*, 276801.
- (37) Valeri, S.; Altieri, S.; del Pennino, U.; di Bona, A.; Luches, P.; Rota, A. Scanning Tunneling Microscopy of MgO Ultrathin Films on Ag(001). *Phys. Rev. B* **2002**, *65*, 245410.
- (38) Baumann, S.; Rau, I. G.; Loth, S.; Lutz, C. P.; Heinrich, A. J. Measuring the Three-dimensional Structure of Ultrathin Insulating Films at the Atomic Scale. *ACS Nano* **2014**, *8*, 1739–1744.
- (39) Berge, S.; Gartland, P.; Slagsvold, B. Photoelectric Work Function of a Molybdenum Single Crystal for the (100), (110), (111), (112), (114), and (332) Faces. *Surf. Sci.* **1974**, *43*, 275–292.
- (40) Pal, J.; Smerieri, M.; Celasco, E.; Savio, L.; Vattuone, L.; Ferrando, R.; Tosoni, S.; Giordano, L.; Pacchioni, G.; Rocca, M. How Growing Conditions and Interfacial Oxygen Affect the Final Morphology of MgO/Ag(100) Films. *J. Phys. Chem. C* **2014**, *118*, 26091–26102.
- (41) Benedetti, S.; Nilius, N.; Myrach, P.; Valenti, I.; Freund, H.-J.; Valeri, S. Spontaneous Oxidation of Mg Atoms at Defect Sites in an MgO Surface. *J. Phys. Chem. C* **2011**, *115*, 3684–3687.
- (42) König, T.; Simon, G. H.; Heinke, L.; Lichtenstein, L.; Heyde, M. Defects in Oxide Surfaces Studied by Atomic Force and Scanning Tunneling Microscopy. *Beilstein J. Nanotechnol* **2011**, *2*, 1–14.
- (43) Nilius, N. Properties of Oxide Thin Films and Their Adsorption Behavior Studied by Scanning Tunneling Microscopy and Conductance Spectroscopy. *Surf. Sci. Rep.* **2009**, *64*, 595–659.
- (44) McKenna, K. P.; Sushko, P. V.; Shluger, A. L. Inside Powders: A Theoretical Model of Interfaces Between MgO Nanocrystallites. *J. Am. Chem. Soc.* **2007**, *129*, 8600–8608.
- (45) McKenna, K. P.; Shluger, A. L. Electron-trapping Polycrystalline Materials with Negative Electron Affinity. *Nat. Mater.* **2008**, *7*, 859–862.